JPE 15-2-13

http://dx.doi.org/10.6113/JPE.2015.15.2.419
ISSN(Print): 1598-2092 / ISSN(Online): 2093-4718

An Improved Flux Estimator for Gap Flux Orientation Control of DC-Excited Synchronous Machines

Yajun Xu† and Jianguo Jiang*

†*Key Laboratory of Control of Power Transmission and Conversion, Ministry of Education, Shanghai Jiao Tong University, Shanghai, China

Abstract

Flux estimation is a significant foundation of high-performance control for DC-excited synchronous motor. For almost all flux estimators, such as the flux estimator based on phase locked loop (PLL), DC drift causes fluctuations in flux magnitude. Furthermore, significant dynamic error may be introduced at transient conditions. To overcome these problems, this paper proposes an improved flux estimator for the PLL-based algorithm. Filters based on the generalized integrator are used to avoid flux fluctuation problems caused by the DC drift at the back electromotive force. Programmable low-pass filters are employed to improve the dynamic performance of the flux estimator, and the cutoff frequency of the filter is determined by the dynamic factor. The algorithm is verified by a 960V/1.6MW industrial prototype. Simulation and experimental results show that the proposed estimator can estimate the flux more accurately than the PLL-based algorithm in a cycloconverter-fed DC-excited synchronous machine vector control system.

Key words: Back electromotive force filter, Flux estimator, Generalized integrator, Phase locked loop, Programmable low-pass filter

I. INTRODUCTION

Flux estimation is very important in implementing high-performance motor drives. For the gap flux orientation vector control system of the synchronous machine, the decoupling effect depends on the accuracy of flux estimation. Motor flux estimator has attracted wide research attention in recent years [1]-[20].

Flux estimation methods based on the motor model are traditional methods, including current model, voltage model, and a combination of both. Among these models, the voltage model is mostly used because of its simple structure and few parameters, especially at high-speed occasions. The traditional voltage model is derived by integrating the back electromotive force (EMF). This model is difficult to apply in practice because of initial phase errors, drift, and saturation problems [1]-[20].

Among these voltage model algorithms, low-pass filter (LPF) is the most commonly used algorithm. To reduce DC drift, the ideal integrator is always approximated by one or several LPFs [3]-[9]. Hurst et al. [3] used causal moving average filters instead of pure integrator. However, this approach resulted in the phase lag and the flux decrease at low speed, which affect the accuracy of flux estimation. Given that the order of the filter is determined by the synchronous frequency, the flux estimator generates dynamic errors at transient conditions.

For estimators based on LPFs that use fixed cutoff frequency, the cutoff frequency is difficult to determine. If the cutoff frequency is high, the DC drift problem can be largely alleviated and the saturation problem can be eliminated. However, the magnitude and angle errors are significant, especially in low-frequency range. Moreover, if the cutoff frequency is low, the drift problem will remain. To solve these problems, the decrement in gain and the phase lag of the LPF can be compensated by multiplying compensators [4]. Given

Manuscript received Jul. 4, 2014; accepted Nov. 18, 2014
Recommended for publication by Associate Editor Sanjeet K. Dwivedi.
†Corresponding Author: star1985star@126.com
Tel: +86-18801966457, Shanghai JiaoTong University
*Key Laboratory of Control of Power Transmission and Conversion, Ministry of Education, Shanghai JiaoTong University, China

that the gain and phase compensator are synchronous frequency-related functions and the synchronous frequency contains a large number of harmonics, such as switching harmonics, compensation values are difficult to calculate accurately. The flux estimator will also worsen at transient conditions.

To improve the performance of the LPF algorithm, Hu et al. [5] proposed a new algorithm. First, the algorithm separates the observed flux magnitude from the phase by Cartesian to Polar coordinate transformation. It then calculates the compensation flux. Finally, the compensation flux changes back to the Cartesian coordinate and compensates the magnitude and phase errors of the LPF by another LPF. With a good PI parameter, this algorithm can estimate the flux in a wide frequency range. However, this method assumes that the back EMF is orthogonal to the flux, which is untrue at transient conditions.

To overcome the problems of fixed frequency LPF, the programmable LPF was proposed [6]-[9]. In general, errors are compensated by the magnitude and phase compensator. The cutoff frequency is adjusted according to the motor synchronous frequency. On the one hand, the cutoff frequency of this algorithm is several times higher than the synchronous frequency, and the drift problem can be largely alleviated. On the other hand, compensation values of the magnitude and phase are constant. Thus, the algorithm can estimate the flux in a wide frequency range. To improve the dynamic performance of the programmable LPF estimator, the cascaded method was proposed [6], [7]. For this algorithm, the programmable single-stage filter is always replaced by two or three programmable cascaded LPFs. However, given that the compensators also contain the synchronous frequency, the results will fluctuate if the actual stator voltages are used to calculate the flux.

Another solution to the drift problem exploits the fact that the offset vector is almost unidirectional, whereas the derivative vector of the circular displacement rotates [10]-[13]. For this method, offset estimators are used to estimate the drift in the EMF, and the results are fed back to the input of the integrator to cancel the drift. This approach essentially belongs to the LPF algorithm. Given that the offset drift is mainly a thermal effect that changes the DC offset very slowly, the response time of the offset estimator is not at all critical [13]. However, the output deviation is large in the process of adjusting. Moreover, the method uses the reference value of the flux, which reduces the accuracy of the algorithm.

An estimation technique based on the principle of the phase locked loop (PLL) was introduced in [14]. This method has a simple structure and can remove the drift considerably. The PLL is also a real-time method. The flux and the synchronous frequency are obtained simultaneously. However, this method assumes that the back EMF is orthogonal to the flux at transient conditions.

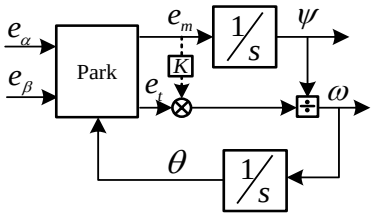

Fig. 1. Block diagram of the flux estimator based on PLL.

Given that the current model always dominates the flux observer at low speeds, the current model can be used to adjust the voltage model [15]-[20]. The current model requires motor parameters and measured motor currents. One of the problems associated with this method is that the parameters change with motor operating conditions.

In these methods, the DC drift is generally incompletely eliminated to solve the saturation problem. In addition, a significant dynamic error may be introduced at transient conditions.

This paper proposes an improved flux estimator for the PLL-based algorithm with back EMF filters and programmable filters. Back EMF filters are used to eliminate the DC drift, and programmable filters are used to enhance the dynamic performance.

II. PLL-Based Flux Estimator

A. The Algorithm

The flux vector is as follows:

$$\boldsymbol{\psi} = \psi e^{j\theta} \tag{1}$$

where θ is the flux angle, and ψ is the magnitude of the flux vector.

According to Faraday's law, the EMF vector can be obtained by the following equation:

$$\boldsymbol{e} = \frac{d\boldsymbol{\psi}}{dt} = \frac{d\psi}{dt} e^{j\theta} + j\omega\psi e^{j\theta} \tag{2}$$

where $\omega = \frac{d\theta}{dt}$ is the synchronous frequency.

The angle of the first part of Eq. (2) is similar to the flux vector. Thus, this part is called the flux-axis component. The magnitude of this part is as follows:

$$e_m = \frac{d\psi}{dt} \tag{3}$$

where m represents the flux axis.

The second part of Eq. (2) is orthogonal to and ahead of the flux axis because of the presence of "*j*." This part is called the torque-axis component. The magnitude of this part is as follows:

$$e_t = \omega\psi \tag{4}$$

where t represents the torque axis.

e_m and e_t can be obtained from e_α and e_β according to the coordinate transformation:

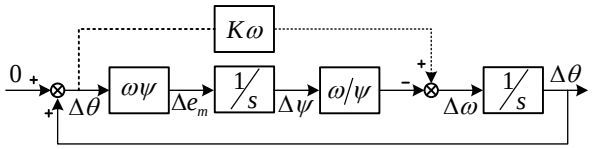

Fig. 2. Small-signal model of the estimator.

$$\begin{cases} e_m = e_\alpha \cos\theta + e_\beta \sin\theta \\ e_t = e_\beta \cos\theta - e_\alpha \sin\theta \end{cases} \tag{5}$$

The block diagram of the motor voltage model based on PLL estimates the flux according to Fig. 1 [14].

Only one parameter occurs in this estimator, namely, *K*, which influences the stability of the estimator.

The principle of this method is that e_m and e_t satisfy Eqs. (3) and (4) respectively when the angle is calculated correctly.

B. Steady-State Error

D_α, D_β are the DC drifts of e_α, e_β respectively. At steady state, these DC drifts produce the error component e_{mD} in e_m.

$$e_{mD} = D_\alpha \cos\theta + D_\beta \sin\theta \tag{6}$$

These DC drifts also cause the error component ψ_D in ψ.

$$\psi_D = \frac{D_\alpha \sin\theta - D_\beta \cos\theta}{\omega} \tag{7}$$

The algorithm cannot completely eliminate the DC drifts, which cause the fluctuation of the flux magnitude.

C. Dynamic-State Error

This method assumes that the back EMF is orthogonal to the flux; hence, e_m is zero. However, this assumption is untrue at transient conditions, especially when the rotor or the stator currents change. These conditions cause changes in flux magnitude, and $\frac{d\psi}{dt}$ may be thousands of times larger than the changes. Therefore, e_m cannot be ignored at transient conditions.

D. Stability of the Estimator

The stability and effectiveness of the algorithm can be verified by the following small-signal analysis method.

Assuming the flux estimator is already stable, more than first-order incremental signals will be neglected.

Assuming the disturbance recently occurred, the flux angle produces errors, namely, $\Delta\theta$. Thus, all the related parameters can be expressed as follows:

$$\begin{cases} \hat{\psi} = \psi + \Delta\psi \\ \hat{\omega} = \omega + \Delta\omega \\ \hat{\theta} = \theta + \Delta\theta \\ \hat{e}_m = e_m + \Delta e_m \\ \hat{e}_t = e_t + \Delta e_t \end{cases} \tag{8}$$

where ^ marks the estimated value, and Ä marks the error between the estimated value and the actual value.

By using Eq. (5), we can obtain

$$\begin{cases} \hat{e}_m = e_t \sin\Delta\theta + e_m \cos\Delta\theta \\ \hat{e}_t = e_t \cos\Delta\theta - e_m \sin\Delta\theta \end{cases} \tag{9}$$

$\cos\Delta\theta \approx 1$ and $\sin\Delta\theta \approx 0$ because $\Delta\theta$ is very small. Eq. (9) can be rewritten as follows:

$$\begin{cases} \Delta e_m = \Delta\theta e_t = \Delta\theta\omega\psi \\ \Delta e_t = -\Delta\theta e_m \end{cases} \tag{10}$$

By using Eqs. (3) and (8), we can obtain

$$\hat{\psi} = \frac{\hat{e}_m}{s} = \frac{e_m + \Delta e_m}{s}$$

Furthermore, we can obtain

$$\Delta\psi = \frac{\Delta e_m}{s} \tag{11}$$

According to Fig. 1 and Eq. (8), the estimated synchronous frequency is as follows:

$$\begin{aligned} \hat{\omega} &= \frac{\hat{e}_t + K\hat{e}_m}{\hat{\psi}} = \frac{e_t + \Delta e_t + K(e_m + \Delta e_m)}{\psi + \Delta\psi} \\ &= \frac{[e_t + \Delta e_t + K(e_m + \Delta e_m)](\psi - \Delta\psi)}{\psi^2 - \Delta\psi^2} \end{aligned} \tag{12}$$

By applying Eqs. (10) to (12), we can express the estimated synchronous frequency as follows:

$$\hat{\omega} = \frac{[e_t - \Delta\theta e_m + K(e_m + \Delta\theta e_t)](\psi - \Delta\psi)}{\psi^2 - \Delta\psi^2} \tag{13}$$

By ignoring all the incremental signals more than the first order, Eq. (13) can be rewritten as follows:

$$\hat{\omega} = \frac{[e_t - \Delta\theta e_m + K(e_m + \Delta\theta e_t)]\psi - (e_t + Ke_m)\Delta\psi}{\psi^2} \tag{14}$$

If the system is running at a constant flux level, $e_m = 0$ can be obtained. In addition, Eq. (14) can be rewritten as follows:

$$\hat{\omega} = \omega + K\omega\Delta\theta - \omega\frac{\Delta\psi}{\psi} \tag{15}$$

We can also obtain

$$\Delta\omega = K\omega\Delta\theta - \omega\frac{\Delta\psi}{\psi} \tag{16}$$

For

$$\hat{\theta} = \frac{\hat{\omega}}{s} = \frac{\omega}{s} + \frac{\Delta\omega}{s} = \theta + \frac{\Delta\omega}{s} \tag{17}$$

Thus,

$$\Delta\theta = \frac{\Delta\omega}{s} \tag{18}$$

Fig. 2 shows the small-signal model of the estimator, which can be obtained through Eqs. (10), (11), (16), and (18).

The close-loop transfer function of the estimator is as follows:

$$f(s) = \frac{-(K\omega - \frac{\omega^2}{s})\frac{1}{s}}{1 - (K\omega - \frac{\omega^2}{s})\frac{1}{s}} = \frac{-K\omega s + \omega^2}{s^2 - K\omega s + \omega^2} \tag{19}$$

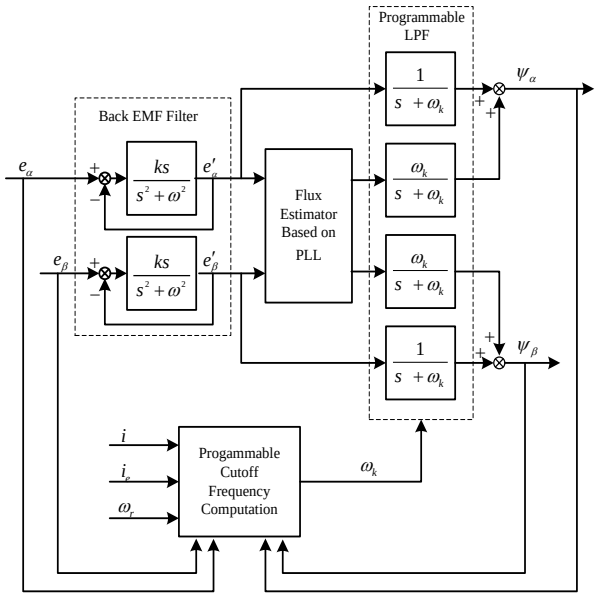

Fig. 3. Block diagram of the proposed estimator.

Based on the Routh stability criterion, the system is stable when

$$K\omega < 0 \tag{20}$$

For example, when $K > 0, \omega < 0$, the roots of the characteristic equation are as follows:

$$\begin{cases} s_{1,2} = \dfrac{K \pm j\sqrt{4-K^2}}{2}\omega & when\ 0 < K < 2 \\ s_{1,2} = \dfrac{K\omega}{2} & when\ K = 2 \\ s_{1,2} = \dfrac{K \pm \sqrt{K^2-4}}{2}\omega & when\ K > 2 \end{cases} \tag{21}$$

According to Eq. (21), the system is under damped when $0 < K < 2$, critically damped when $K = 2$, and over damped when $K > 2$.

III. Proposed Flux Estimator

This paper proposes an improved flux estimator for PLL-based algorithms with back EMF filters and programmable filters. Fig. 3 shows the block diagram of the proposed flux estimator. Back EMF filters are used to completely eliminate the DC drift, and programmable filters are used to enhance the dynamic performance.

A. Back EMF Filter

In the stationary $\alpha - \beta$ reference frame, the air-gap flux is derived by integrating the back EMF $e = u - Ri - L_\sigma \dfrac{di}{dt}$, which yields

$$\psi = \int (u - Ri - L_\sigma \frac{di}{dt})dt \tag{22}$$

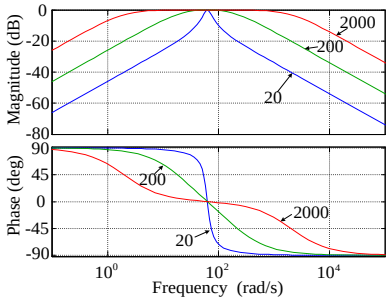

Fig. 4. Frequency characteristics of the EMF filters.

where R is the stator resistance, L_σ is the stator leakage inductance, u is the stator voltages, i is the stator currents, and ψ is the gap flux.

The EMF, which is calculated by Eq. (22), contains high-frequency component harmonics, such as switching harmonics, and a DC drift, which is unavoidable in the analog sampling process. In general, the first-order high-pass filter (HPF) is used to remove the DC drift, which causes magnitude and phase errors. This paper uses a new back EMF filter based on a generalized integrator (Fig. 3). This filter uses a negative feedback loop of EMF. Taking the α axis for example, the output of the generalized integrator e'_α is an alternating signal. If errors are found between the output of the generalized integrator and the fundamental component of e_α, the generalized integrator will work and errors will be eliminated. Thus, the fundamental component of e_α, e'_α, is obtained. The most important factor of this method is k. The way to select the value of k will be illustrated later. To obtain the correct flux, the resonant frequency of the generalized integration is also equal to the synchronous frequency of the machine.

The close-loop transfer function of the back EMF filter is given by

$$\frac{e'_\alpha(s)}{e_\alpha(s)} = \frac{ks}{s^2 + ks + \omega^2} \tag{23}$$

The DC gain of this filter is zero. Thus, this filter can effectively suppress the DC signal.

The gain of fundamental frequency is as follows:

$$\frac{e'_\alpha(j\omega)}{e_\alpha(j\omega)} = \frac{kj\omega}{-\omega^2 + kj\omega + \omega^2} = 1 + j0 \tag{24}$$

Hence, this back EMF filter can track the synchronous frequency component without errors in both magnitude and phase.

For the proposed filter strategy, the crucial question is how to determine the value of proportional gain k. The value of k influences the process of extracting the synchronous component of the EMF. Fig. 4 shows the Bode plot responses for the filter with different values of gain k, such as 20, 200, and 2000. The resonant frequency of the generalized

integration is 62.83 rad/s. In addition, regardless of the value of k, the magnitude response is 0 dB and the phase response is 0° at the resonant frequency. This result confirms that the value of k has no effect at steady state. At transient conditions, the larger the value of k, the greater the magnitude response. Therefore, the larger the value of k, the better the dynamic performance. Thus, to ensure the dynamic performance, the value of k is at least 1000.

B. Flux Observer with Programmable Filters

The Laplace transform of Eq. (22) is as follows:

$$\psi(s)=\frac{1}{s}e(s)=\frac{1}{s}e(s)\frac{s+\omega_k}{s+\omega_k} \tag{25}$$

The term in the right is expanded by a fraction unity value. The expression is then decomposed as follows:

$$\psi(s)=\frac{1}{s+\omega_k}e(s)+\frac{\omega_k}{s+\omega_k}\psi_{PLL}=\psi_1+\psi_2 \tag{26}$$

The result is the equivalent of the pure integral of e on the condition that $\psi=\psi_{PLL}$. ψ_1 is obtained by the most common method, namely, the first-order LPF method. This method is the traditional pure integration algorithm essentially cascaded with an HPF. Thus, the higher the input frequency (or the lower the cutoff frequency), the greater the ψ_1. ψ_2 is obtained by the flux estimator based on PLL cascaded with an LPF. Thus, the higher the input frequency (or the lower the cutoff frequency), the smaller the ψ_2.

The structure of pure integration is simple, and the estimating result is accurate at high speed. Furthermore, the flux estimator based on PLL has good performance at steady state but dynamic errors at transient conditions. Therefore, the proportion of ψ_1 should be as large as possible at transient conditions by reducing ω_k, which improves the accuracy of dynamic flux estimation. Considering the dynamic integration error problem, ω_k is usually greater than zero. To eliminate errors caused by the DC drift and the disturbance, ω_k is equal to the synchronous frequency of the machine at steady state.

C. Implementation of the Programmable LPF

The continuous-time transfer function of the programmable LPF can be converted to discrete-time form by the Euler method [21]:

$$s=\frac{1-z^{-1}}{T_s} \tag{27}$$

where T_s is the sampling period of the discrete system.

Combining Eqs. (26) and (27) result in the following discrete-time transfer function of the programmable LPF:

$$\psi(z)=\frac{T_s}{1-z^{-1}+\omega_k T_s}e(z)+\frac{\omega_k T_s}{1-z^{-1}+\omega_k T_s}\psi_{PLL} \tag{28}$$

D. Obtaining Programmable Frequency ω_k

In terms of improving dynamic performance, the proposed algorithm is mainly dependent on the programmable frequency, which is changed based on the base cutoff frequency. The base cutoff frequency can be calculated by

$$\omega_{kb}=\frac{e_\beta\psi_\alpha-e_\alpha\psi_\beta}{|\psi|^2} \tag{29}$$

The dynamic factor d and the programmable frequency ω_k' are given as follows:

$$d(s)=\frac{\tau_1 i(s)+\tau_2 i_e(s)+\tau_3\omega_r(s)}{\tau_1+\tau_2+\tau_3}\frac{s}{\tau_i s+1} \tag{30}$$

$$\omega_k'=\begin{cases}\omega_{kb} & d\le d_{\min}\\ \dfrac{\omega_{k0}-\omega_{kb}}{d_{\max}-d_{\min}}(d-d_{\min}) & d_{\min}<d<d_{\max}\\ \omega_{k0} & d\ge d_{\max}\end{cases} \tag{31}$$

where τ_1, τ_2, τ_3, and τ_i are the time constants; ω_{k0} is the minimum frequency; and $d_{\min}$ and $d_{\max}$ are the threshold of the dynamic factor.

To reduce the disturbances, the programmable frequency ω_k is obtained by filtering ω_k' with a first-order LPF, and the cutoff frequency of the LPF is ω_d.

E. Effects of Parameter Variation

Parameter variation of the synchronous machine is caused by the various operating conditions, such as ambient temperature and flux level. The robustness to the parameter variation is requisite for practical estimation in the flux estimator. For the presented method, the results of Eq. (22), flux estimator based on PLL, and Eq. (26) are essentially derived by integrating the back EMF.

From Eq. (22), the actual flux is as follows:

$$\psi=\frac{u-Ri}{s}-L_\sigma i \tag{32}$$

The flux with parameter errors is as follows:

$$\hat{\psi}=\frac{u-\hat{R}i}{s}-\hat{L}_\sigma i \tag{33}$$

If $\hat{R}=1.5R$, the flux error is as follows:

$$\Delta\psi=\hat{\psi}-\psi=\frac{-0.5Ri}{j\omega} \tag{34}$$

The estimated flux error caused by the parameter (R) uncertainties is shown in Fig. 5. In the figure, both the stator current and the rated flux are 1 pu.

Moreover, as the synchronous speed increases, estimated flux error decreases because the magnitude of back EMF increases and the flux error is proportional to the stator current.

If $\hat{L}_\sigma=1.5L_\sigma$, then the flux error is as follows:

$$\Delta\psi=\hat{\psi}-\psi=-0.5L_\sigma i \tag{35}$$

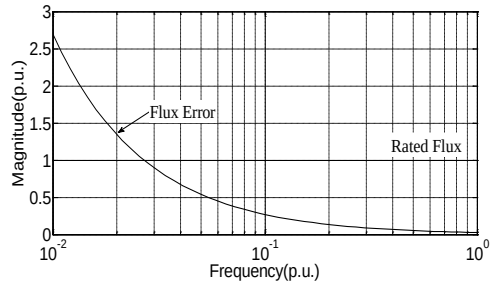

Fig. 5. Magnitude errors of the flux estimator.

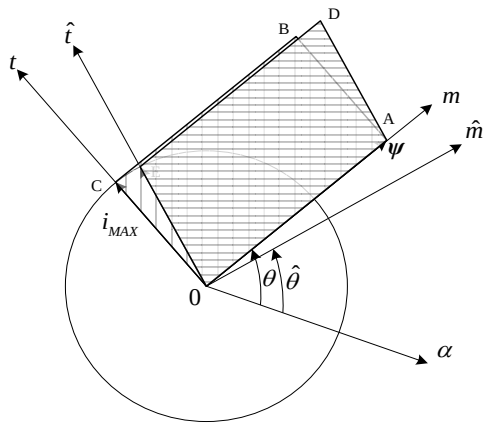

Fig. 6. Influence of estimated flux angle on the maximum output torque.

In Eq. (35), no relationship is found between the flux error and the synchronous speed. However, the flux error is proportional to the stator current.

At steady state, the flux magnitude and synchronous frequency are determined by the flux estimator based on PLL. Given that the parameters change gradually and affect both e_α and e_β, the parameter variation will not cause the change in synchronous frequency. From Eq. (4) and $e_m = 0$, the flux error is as follows:

$$\Delta\psi' = \frac{\hat{e}_t - e_t}{\omega}\frac{1}{j} = -\frac{(\hat{R} - R)}{j\omega}i - (\hat{L}_\sigma - L_\sigma)i \tag{36}$$

Eq. (36) is consistent with Eqs. (34) and (35).

F. Effects on Control Results

The flux estimator has an effect on the controllers and regulators because flux accuracy affects the decoupling effect of the system. Assuming the actual value of the flux angle is θ and the angle containing the error is $\hat{\theta}$, Fig. 6 shows the influence of estimated flux angle on the maximum output torque. The circle represents the maximum stator current. The area of rectangular 0ABC represents the maximum torque generated by the maximum current when the flux is estimated correctly. If an error is found in the estimated angle such as $\hat{\theta}$, then the area of the quadrilateral (represents the torque), 0ADE, is smaller than 0ABC. The smaller the area, the smaller the torque.

TABLE I
MOTOR SPECIFICATIONS

Rated power	1600000W
Stator voltage	2×960 V
Stator current	2×517.3 A
Frequency	7.167 Hz
Rotor speed	43 rpm
Phase	2×3
Rotor current	289.6 A
Stator resistance	0.0539 pu
Leakage reactance of stator	0.1638 pu
Resistance of excitation winding	0.01486 pu
Main leakage reactance to d-direction	1.806 pu
Main leakage reactance to q-direction	1.009 pu
Sampling Period for Vector Control	0.00167s
Sampling Period for Phase Control	0.00033s

The torque needed for the acceleration of the rotating body is as follows:

$$T_d - T_L = \frac{d}{dt}(J\omega_r) \tag{37}$$

where T_d is the torque provided by the machine, T_L is the torque of the load, J is the moment of inertia, and ω_r is the rotor speed.

In Eq. (37), if the machine cannot provide enough torque, then the machine will not reach the required speed.

IV. SIMULATION RESULTS

To evaluate the performance of the proposed scheme, a simulation model is established using Matlab/Simulink. The main motor parameters are shown in Table I. The armature of the synchronous motor, originally with a conventional three-phase single-star arrangement, is rewound to obtain two 30 electrical degrees spatially shifted three-phase star windings. The synchronous motor is fed by a cycloconverter, which works in a non-circulating current mode. The dead time is 0.002 s.

A. Performance of the Back EMF Filter

To test the back EMF filter, a 0.5 V DC voltage was added to the alpha axis of the EMF at 4ths in a step fashion. The DC drifts cause the fluctuation of the flux magnitude [Fig. 7(a)], which is consistent with the analysis in Section II. With the back EMF filter, the fluctuation amplitude gradually decays. The filter causes a 0.0005 s delay [Figs. 7(b) and 7(c)]. This phenomenon is the main drawback of the scheme. Fortunately, the delay can be reduced by a compensator.

B. Performance at Transient Conditions

To verify the proposed flux estimator at transient conditions, simulations with the step changes of rotor current, stator current, and speed were conducted.

To test the behavior of the proposed flux estimator when the rotor current changes, the rotor flux-oriented vector control is

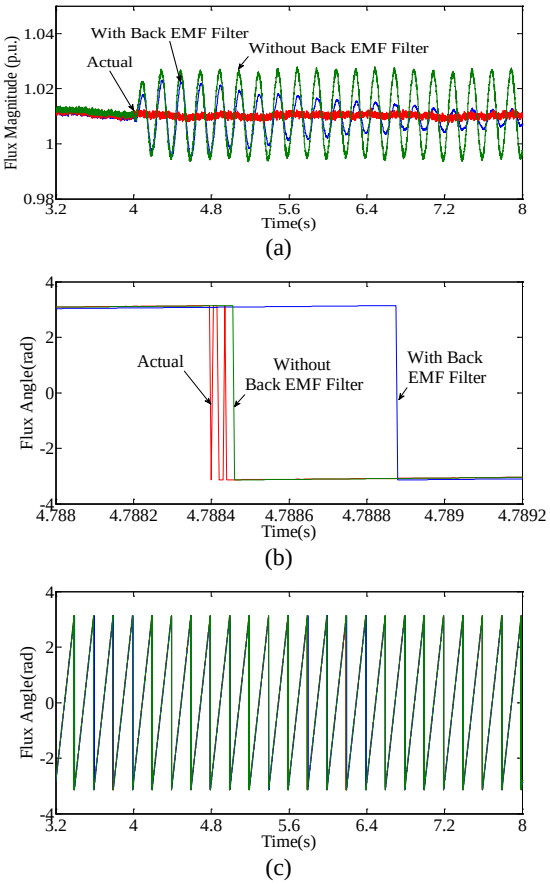

Fig. 7. Step change of the DC drift. (a) Flux magnitude. (b) Flux angle. (c) Flux angle with time zoom.

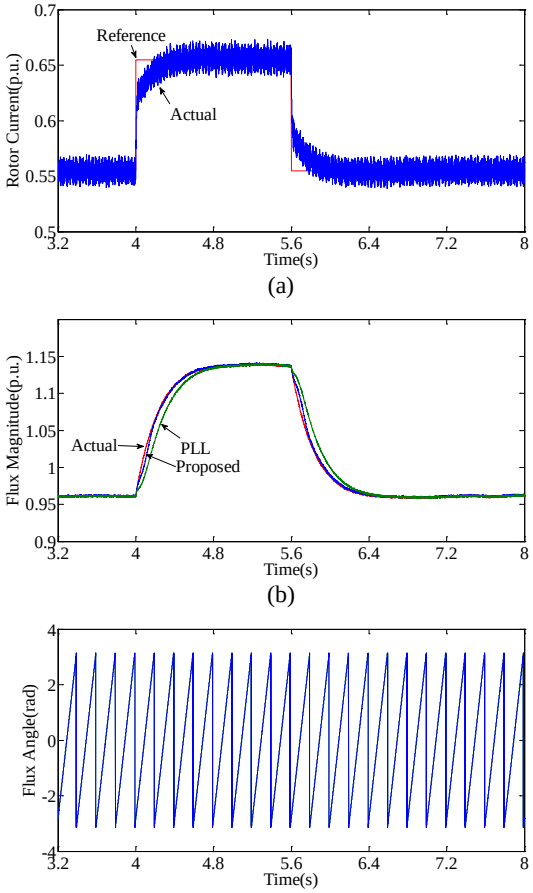

Fig. 8. Step change of the rotor current. (a) Rotor current. (b) Flux magnitude. (c) Flux angle.

used in the system. Figs. 8(b) and 8(c) illustrate the transient response of the flux at no load for step reference rotor current change from 0.555 pu to 0.655 pu, and then back to 0.555 pu. For synchronous motors, the stator current is almost zero at no load. Thus, the flux change is largely determined by the change of the rotor current. The flux magnitude of the PLL-based algorithm has a significant error when the rotor current changes and the error of the proposed algorithm is small [Fig. 8(b)]. Both estimation algorithms can accurately estimate the flux angle when the rotor current changes, because the deviation between the flux angle and the rotor position angle is determined by the load current, which is almost zero for this simulation.

To test the behavior of the proposed flux estimator when the stator current changes, the gap flux -oriented vector control is used to in the system. In addition, the rotor current also follows the stator currents. Fig. 9 shows the transient responses at 31.4 rad/s for step variation of the load torque from 0 pu to 1 pu, and then back to 0 pu. Errors are found between the actual flux magnitude and the magnitude estimated by the PLL-based algorithm ([Fig. 9(b)]). However, the errors of the proposed algorithm are small. The zoomed angle in Fig. 9(d) illustrates that the angle errors of the PLL-based algorithm are much larger than those of the proposed algorithm. Moreover, the waveforms of the proposed algorithm are smoother than the actual value. This result is because of the role of the back EMF filter.

Fig. 10 illustrates the transient behavior at no load for reference speed change from 0.4 pu to 0.3 pu, and then back to 0.4 pu. The speed, stator currents, and rotor current all change at transient conditions. Flux magnitude of the PLL-based algorithm has a significant error when the speed changes, and the proposed algorithm has only small errors [Fig. 10(b)]. The zoomed angle in Fig. 10(d) illustrates that the angle errors of the PLL-based algorithm are much larger than the proposed algorithm. The largest estimation errors of the proposed algorithm occurred at the mid-transition process of the flux. This phenomenon is due to the dynamic state process of the speed and currents have basically ended and the flux is mainly obtained by the PLL part, but this part still has errors.

V. Experimental Results

The synchronous motor drive with a flux estimator based on the proposed algorithm is implemented in an industrial prototype. All the experimental results in this paper are obtained through this industrial prototype. The parameters of

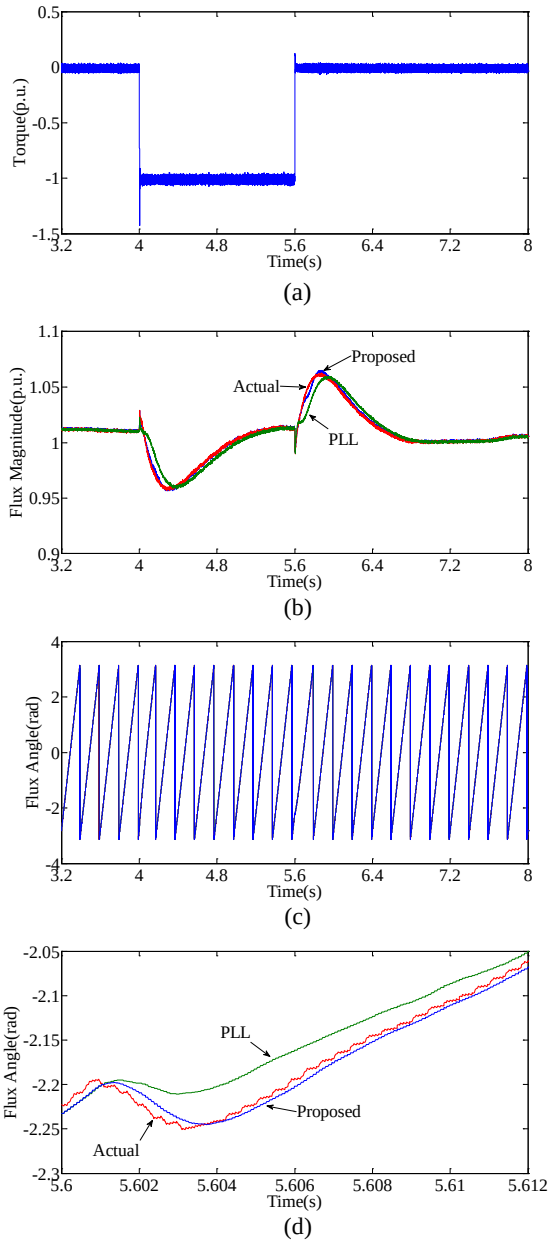

Fig. 9. Step change of the torque. (a) Torque. (b) Flux magnitude. (c) Flux angle. (d) Flux angle with time zoom.

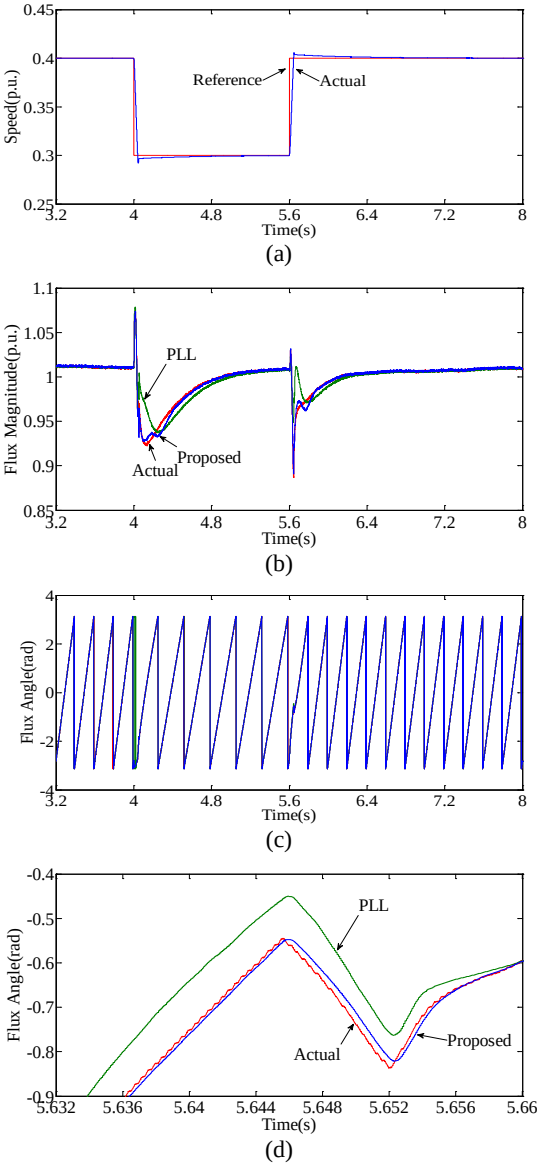

Fig. 10. Step change of the speed. (a) Speed. (b) Flux magnitude. (c) Flux angle. (d) Flux angle with time zoom.

the double-star electrical excitation motor used in the experiments are shown in Table I. Fig. 11 shows the digital controller of the industrial prototype. The architecture of multi-CPU and VersaModule Europe bus are used to control the system. The controller includes a CPU board, a digital in/out board, a digital-to-analog (DA) board, a Profibus board, and six phase control boards. Speed control, flux control, excitation current control, and vector control are implemented in the CPU board. The phase control boards are used to control the alternating stator current of each phase. Each phase control board is responsible for the discontinuous current compensation, the switching logic of the non-circulating current mode, and pulse firing. To observe the internal variables conveniently,

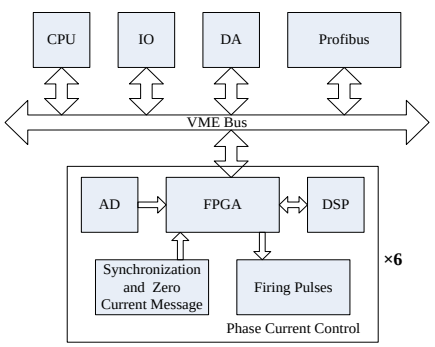

Fig. 11. Digital Controller.

real-time displays of the estimator outputs are implemented by DA, and the output frequency is 1 kHz. Fig. 12 shows the images of the industrial prototype used in the experiment. The stator currents of the machine are measured by CHB-1000S,

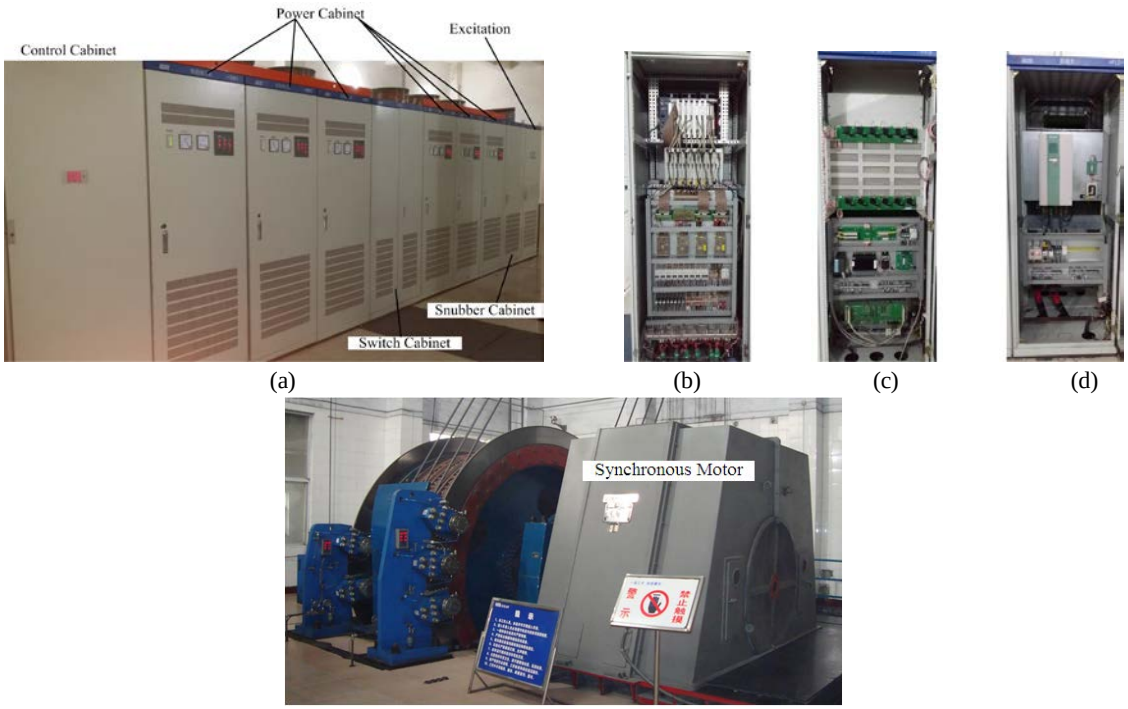

Fig. 12. Images of the industrial prototype. (a) Control and power cabinet. (b) Control cabinet. (c) Power cabinet. (d) Excitation cabinet. (e) Synchronous motor.

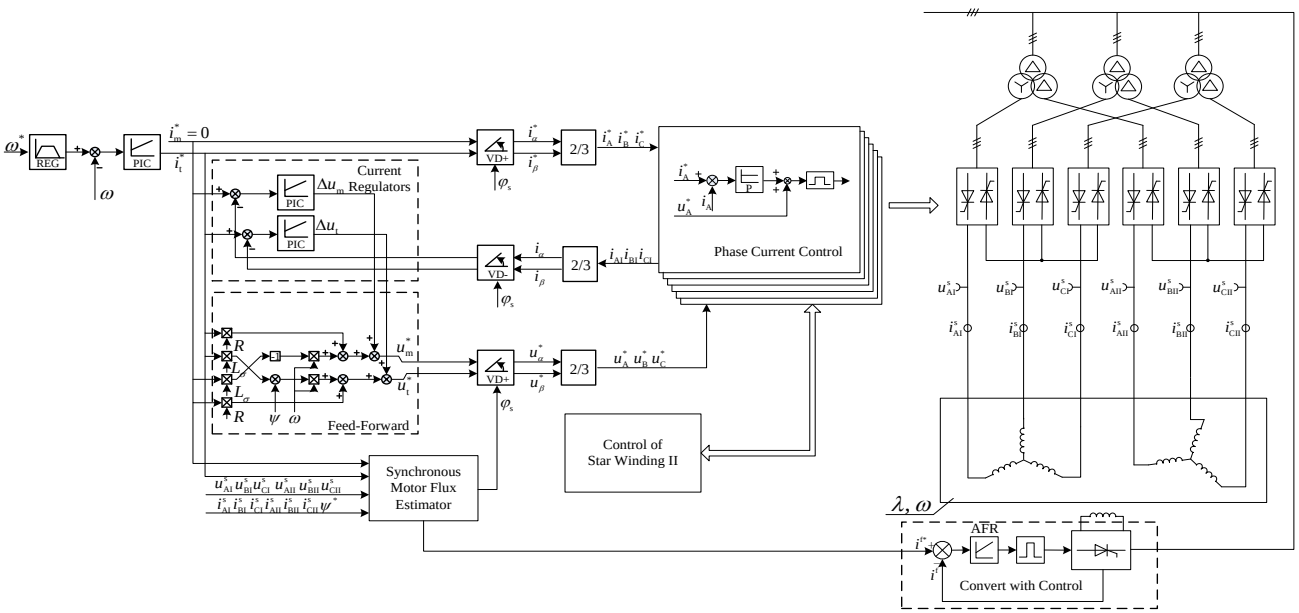

Fig. 13. Block diagram of the industrial prototype.

and its stator voltages are measured by LV100. Fig. 13 shows the block diagram of the industrial prototype, which is a cycloconverter-fed double-star synchronous motor vector control system.

To test the behavior of the proposed back EMF filter, the rotor flux-oriented vector control is used in the system.

Fig. 14 illustrates the transient behavior at no load for step reference rotor current change from 0.56 pu to 0.4 pu, and then back to 0.56 pu. Compared with the waveforms of rotor current i_e and the flux ψ without the back EMF filters shown in Fig. 14(a), Fig. 14(b) shows waveforms that use the back EMF filters. From the figure, the fluctuations of the flux magnitude are significantly reduced by the filters, and the filters have minor effect on the dynamic response of the flux.

Figs. 15 and 16 show the experimental performance of the various flux estimators for the equally demanding conditions

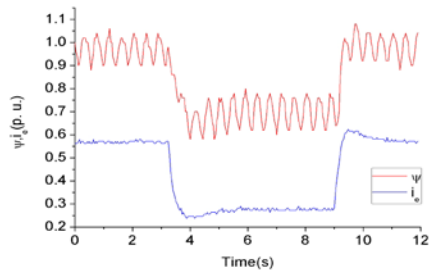

(a)

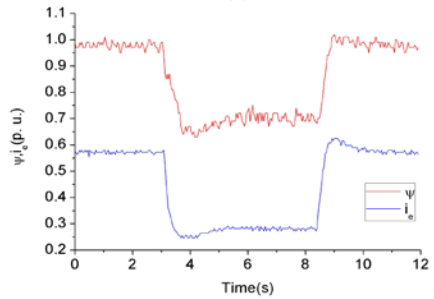

(b)

Fig. 14. Experimental result with step change of the rotor current. (a) Without the back EMF filter. (b) With the back EMF filter.

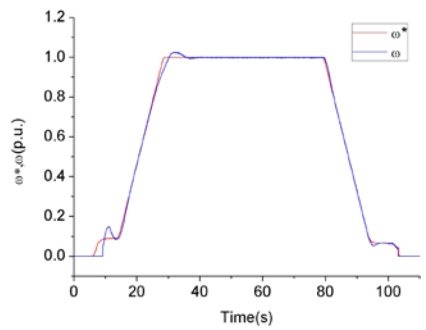

(a)

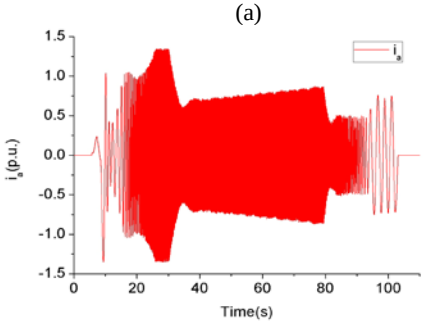

(b)

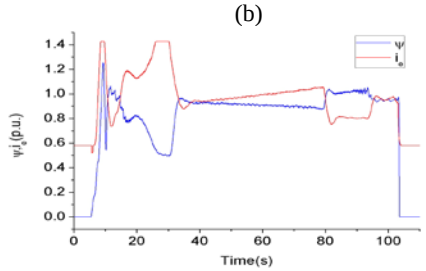

(c)

Fig. 15. Experiment results with the flux estimator based on PLL. (a) Speed. (b) Stator current of one phase. (c) Flux and rotor current.

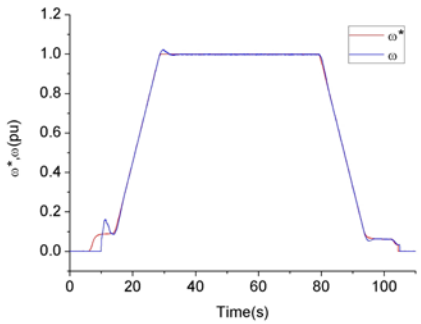

(a)

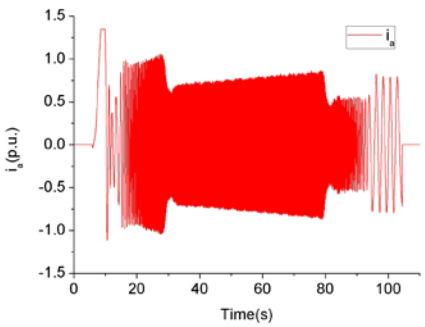

(b)

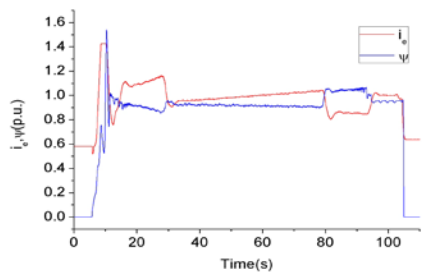

(c)

Fig.16. Experiment results with the proposed flux estimator. (a) Speed. (b) Stator current of one phase. (c) Flux and rotor current.

of the reference speed (ω^*) change from 0% to 100%, and then back to 0% at constant 100% torque. Furthermore, the maximum torque is limited to ±135%. In the final stage of the acceleration, the power demand is at the maximum, and the speed error of the PLL-based algorithm is greater than that of the proposed algorithm [Figs. 15(a) and 16(a)]. The stator and rotor currents of the system based on proposed flux estimator are smaller than the system based on the PLL flux estimator in the final stage of the acceleration [Figs 15(b), 16(b), 15(c), and 16(c)]. From the analysis of Section III part F and Figs. 15(b) and 16(b), the more accurate the angle, the greater the torque at the same current level. The proposed algorithm uses less current and reaches better control effect than the PLL-based algorithm. This result is enough to prove that the flux obtained by the proposed algorithm is more accurate than that obtained by the PLL-based algorithm.

The flux magnitude reduces as the stator current increases [(Figs. 15(b) and 15(c)]. Therefore, the estimated flux is inaccurate and affects the decoupling effect of the current

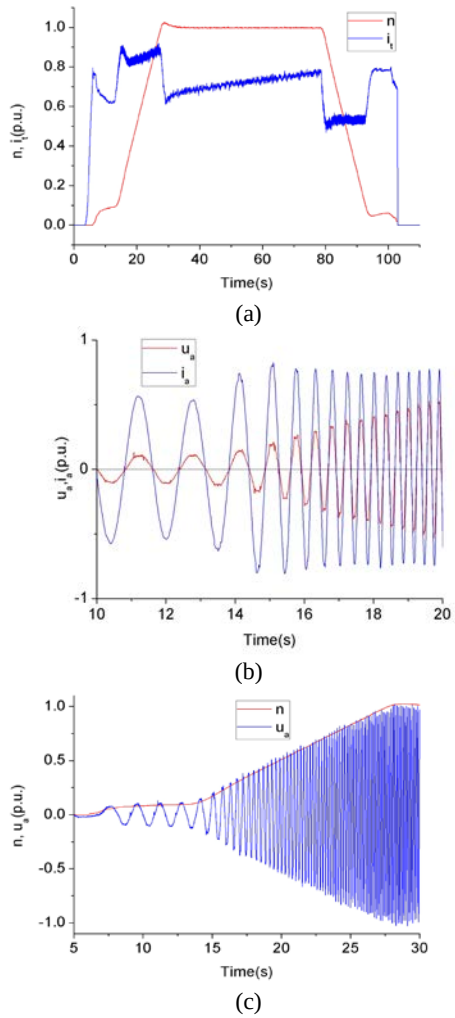

Fig.17. Extended experiment results with the proposed method. (a) Speed and torque current. (b) Stator voltage and current of one phase. (c) Speed and stator voltage of one phase.

controller at transient conditions.

Fig. 17 shows the extended experiment results with the proposed flux estimator. The only difference is that the brake release time of Fig. 17 is earlier than that of Fig. 16. The voltage and current phase are coherent, indicating that reactive current (flux component) is small [Fig. 17(b)]. The voltage is proportional to the speed, indicating that the magnitude of the flux changes slightly [Fig. 17(c)].

VI. CONCLUSIONS

This paper investigates the DC drift problem and dynamic errors of the gap flux estimation for DC-excited synchronous machines. The DC drift causes fluctuations of the flux based on analytical and experimental analyses. The back EMF filter based on generalized integrator is used to solve this problem. The fluctuations are greatly reduced by this approach. The results of the PLL-based estimator are inaccurate and it affects the decoupling effect of the current controller at transient conditions. Programmable LPFs are employed to improve the dynamic performance of the flux estimator. Compared with the PLL-based flux estimator, the proposed algorithm can estimate the flux more accurately at transient conditions, where the stator current and the rotor current required for the system are smaller under the same conditions.

ACKNOWLEDGMENT

The authors appreciate the financial supports provided by the National High Technology Research and Development Program of China (863 Program), Grant No. 2011AA050403.

REFERENCES

[1] H. U. Rehman, “Design of voltage model flux observer,” *IEE Proc. Electr. Power Appl*, Vol. 151, No. 2, pp. 129-134, 2004.

[2] R. Rodríguez, R. A. Gómez, and J. Rodríguez, “Fast square root calculation for DTC magnetic flux estimator,” *IEEE Latin America Transactions*, Vol. 12, No. 2, pp.112-115, Mar. 2014.

[3] K. D. Hurst, T. G. Habetler, G. Griva, and F. Profumo, “Zero-speed tacholess IM torque control: Simply a matter of stator voltage integration,” *IEEE Trans. Ind. Appl.*, Vol. 34, No. 4, pp. 790-795, Jul./Aug. 1998.

[4] N. R. N. Idris and A. H. M. Yatim, “An improved stator flux estimation in steady-state operation for direct torque control of induction machines,” *IEEE Trans. Ind. Appl.*, Vol. 38, No. 1, pp. 110-116, Jan./Feb. 2002.

[5] J. Hu and B. Wu, “New integration algorithms for estimating motor flux over a wide speed range,” *IEEE Trans. Power Electron.*, Vol. 13, No. 5, pp. 969-977, Sep. 1998.

[6] B. K. Bose and N. R. Patel, “A programmable cascaded low-pass filter-based flux synthesis for a stator flux-oriented vector-controlled induction motor drive,” *IEEE Trans. Ind. Electron.*, Vol. 44, No. 1, pp. 140-143, Feb. 1997.

[7] B. Karanayil, M. F. Rahman, and C. Grantham, “An implementation of a programmable cascaded low-pass filter for a rotor flux synthesizer for an induction motor drive,” *IEEE Trans. Power Electron.*, Vol. 19, No. 2, pp. 257-263, Mar. 2004.

[8] S.-S. Lee, B.-G. Park, R.-Y. Kim, and D.-S. Hyun, “Improved stator flux estimator based on a Programmable LPF for sensorless control of induction motors,” *IEEE Industry Applications Society Annual Meeting (IAS)*, pp. 1-8, 2012.

[9] A. Ghaderi and T. Hanamoto, “Wide-speed-range sensorless vector control of synchronous reluctance motors based on extended programmable cascaded low-pass filters,” *IEEE Trans. Ind. Electron.*, Vol. 58, No. 6, pp. 2322-2333, Jun. 2011.

[10] Q. Gao, C. S. Staines, G. M. Asher, and M. Sumner, “Sensorless speed operation of cage induction motor using zero drift feedback integration with MRAS observer,” in *2005 European Conference on Power Electronics and Applications*, pp. 1-9, 2005.

[11] J. Holtz, “Sensorless control of induction machines-with or without Signal Injection?,” *IEEE Trans. Ind. Electron.*,

Vol. 53, No. 1, pp. 7-30, Feb. 2006.
[12] J. Holtz and J. Quan, "Sensorless vector control of induction motors at very low speed using nonlinear inverter model and parameter identification," *IEEE Trans. Ind. Appl.*, Vol. 38, No. 4, pp. 1087-1095, Jul./Aug. 2002.
[13] J. Holtz and J. Quan, "Drift- and parameter-compensated flux estimator for persistent zero-stator-frequency operation of sensorless-controlled induction motors," *IEEE Trans. Ind. Appl.*, Vol. 39, No. 4, pp. 1052-1060, Jul./Aug. 2003.
[14] X. Wei and X. Ma, "Some techniques of vector control systems of medium voltage three level inverters," in *Power Electronics and Motion Control Conference*, pp. 1399-1403, 2004.
[15] I. Boldea, M. C. Paicu, and G.-D. Andreescu, "Active flux concept for motion-sensorless unified AC drives," *IEEE Trans. Power Electron.*, Vol. 23, No. 5, pp. 2612-2618, Sep. 2008.
[16] P. L. Jansen and R. D. Lorenz, "A physically insightful approach to the design and accuracy assessment of flux observers for field oriented induction machine drives," *IEEE Trans. Ind. Appl.*, Vol. 30, No. 1, pp. 101-110, Jan./Feb. 1994.
[17] A. Aimad, K. Madjid, and S. Mekhilef, "Robust sensorless sliding mode flux observer for DTC-SVM-based drive with inverter nonlinearity compensation," *Journal of Power Electronics*, Vol. 14, No. 1, pp. 125-134, Jan. 2014.
[18] V. Coroban-Schramel, I. Boldea, G.-D. Andreescu, and F. Blaabjerg, "Active-flux-based motion-sensorless vector control of biaxial excitation generator/motor for automobiles," *IEEE Trans. Ind. Appl.*, Vol. 47, No. 2, pp. 812-819, Mar./Apr. 2011.
[19] J.-H. Kim, J.-W. Choi, and S.-K. Sul, "Novel rotor-flux observer using observer characteristic function in complex vector space for field-oriented induction motor drives," *IEEE Trans. Ind. Appl.*, Vol. 38, No. 5, pp. 1334-1343, Sep./Oct. 2002.
[20] C. I. Pitic, G.-D. Andreescu, F. Blaabjerg, and I. Boldea, "IPMSM motion-sensorless direct torque and flux control," in *31st Annual Conference of IEEE Industrial Electronics Society (IECON 2005)*, pp. 1756-1761, 2005.
[21] G. Ellis, *Control System Design Guide*, Elsevier Academic Press, Chap. 5, 2004.

Yajun Xu was born in Xuzhou, China. He received his B.S. and M.S. degrees in Electrical Engineering in 2007 and 2010 respectively from China University of Mining and Technology, Xuzhou, China. He is currently working toward his Ph.D. at the Key Laboratory of Control of Power Transmission and Conversion, Shanghai Jiao Tong University, Shanghai, China. His current research interests include cycloconverter and synchronous motor control.

Jianguo Jiang was born in 1956 in China. He received his Ph.D. degree in Electrical Engineering in 1988 from China University of Mining and Technology, Xuzhou, China. He is currently a Professor of Electrical Engineering at Shanghai Jiao Tong University, Shanghai, China. His current research interests include high-power converters, power quality, and motor control.